

# Optimization of reaction kinetics on natural convection microfluidic devices by computer simulation

L. C. Olivares-Rueda\*, C. Mendoza-Barrera, A. Y. Tenorio-Barajas, S. Muñoz-Aguirre, M. Rodríguez-Torres, and V. Altuzar\*

*Facultad de Ciencias Físico-Matemáticas, Benemérita Universidad Autónoma de Puebla,  
Puebla 72570, México*

*e-mail: \*luis.olivares616@outlook.com; \*valtuzar@fcfm.buap.mx*

Received 2 January 2024; accepted 7 March 2024

This study presents a novel methodology framework for simulating and optimizing reaction kinetics in natural convection microfluidic devices. The approach involves coupling heat and mass transfer, fluid flow, and chemistry. Visual and regression analyses are performed to evaluate the impact of different operational parameters on reaction speed, aiming to improve microfluidic natural convection systems. The methodology was applied to a practical example of a Polymerase Chain Reaction in an triangular microfluidic glass device that utilizes natural convection for the required reactions. The findings showed that the fluid flow velocity is significant in determining the reaction speed, which can be controlled by adjusting the temperature cycling differences and the inner diameter of the device. Despite challenges posed by the fluid flow direction, the best reaction times achieved ranged from 18 to 21 minutes. Due to its computational efficiency, the developed methodology allows simulations to be conducted on mid-range computers. Also, the visual and regression analyses offer insights into improving a specific device by measuring the influence of several parameters. Then, the methodology is convenient for selecting the best conditions before developing an experiment.

**Keywords:** Computational simulation; methodology; microfluidic natural convection system; PCR.

DOI: <https://doi.org/10.31349/RevMexFis.70.041003>

## 1. Introduction

Natural convection systems play a significant role in chemical reactions, especially those involving heat transfer like the Polymerase Chain Reaction (PCR) used in disease detection [1,2]. These systems facilitate mixing [3], mass transfer, and temperature control [3,4]. Natural convection occurs due to density differences resulting from temperature variations in a fluid. When a fluid is heated, it becomes less dense; meanwhile, if it is cooler, it is denser. Microfluidic technology offers a significant advantage over traditional heater devices, including compact dimensions, reduced reactant volumes, and simplified and rapid temperature control [5,6]. However, the design of efficient microfluidic devices demands considerable time and effort. Computer simulation is an indispensable tool for designing and optimizing natural convection microfluidic devices to accelerate this process [6-8]. Contrary to what is commonly thought, natural convection in microfluidic devices has been shown to have significant effects that cannot be negligible [3,8]. Several approaches have been successfully used for simulating reactions in microfluidic devices, such as stochastic modeling for a more accurate simulation of reaction kinetics [9] and the usage of automatic control for the temperatures on those devices in the simulations via a connection with a programming language [10]. Multi-physics approaches are needed to simulate reactions in a natural convection device. Papadopoulos *et al.* [10] and Wang *et al.* [11] used a multi-physics approach to simulate the reaction kinetics of a continuous flow device where the materials needed for a reaction are injected through a channel. Meanwhile, heat is passively applied in specific zones to effectuate

the chemical reactions as the material advances through the channel. This type of device is like a natural convection one. The main difference is how the flow of the material is generated and the shape of the channels. Several authors have simulated and crafted natural convection devices with channels that form closed loops. Heat applied in different zones causes the generation of a flow due to the difference in densities and the temperature gradients. Priye *et al.* studied natural convection reactions introducing turbulence [12]. In contrast, Agrawal *et al.* crafted several natural convection microfluidic devices after simulating the flows generated by applying heat and not considering the presence of reactants and reactions in the simulations [4,8]. Also, simulations involving reactions on natural convection systems at large scales have been done before [13], but convection or reaction kinetics are commonly included separately for microfluidic devices. In addition, some authors include automatic control of temperatures or tested some devices. Still, a methodology must be applied to quantitatively measure the impact of the temperatures and the temperature differences for a particular device.

### 1.1. Polymerase chain reaction

The polymerase chain reaction (PCR) is a highly utilized technique in medical genetics and various fields of biological science. It involves amplifying specific deoxyribonucleic acid (DNA) fragments (amplicons) by subjecting a reaction mixture of nucleic acids to thermal cycling. The mixture

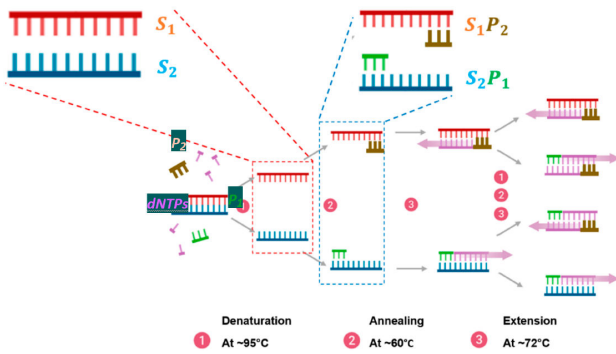


FIGURE 1. The PCR reaction involves amplifying specific amplicons by subjecting a reaction of deoxynucleotide triphosphates, DNA polymerases, and DNA samples containing the target to thermal cycles. The sequential cycles of denaturation (heating the mixture to denature the double-stranded DNA or ssDNA), annealing (cooling of the mixture to bind the primers to form stable primer-ssDNA complexes), and extension (synthesis of the complementary DNA strands by extending the primers) are carried out until the amplification of the target DNA sequence is reached. Adapted image from [17].

consists of oligonucleotide primers complementary to the DNA sequences of interest, deoxynucleotide triphosphates (dNTPs), DNA polymerases, and DNA samples containing the target sequence. The core cycle of the PCR includes 1. denaturation, 2. annealing, and 3. extension, which is repeated multiple times to achieve amplification of the target DNA sequence [14-16] (Fig. 1). The denaturation involves heating the mixture ( $95^{\circ}\text{C}$ ) to separate (denaturation) the double-stranded DNA (dsDNA or  $S_1S_2$ ) into two separate single-stranded DNA (ssDNA or  $S_1$  and  $S_2$ ) strands. During the annealing, the mixture is cooled ( $55^{\circ}\text{C}$ ) to bind the oligonucleotide primers ( $P_1$  and  $P_2$ ) to the complementary DNA sequences on the ssDNA, forming stable primer-ssDNA complexes ( $S_1P_2$  and  $S_2P_1$ ). Finally, the extension includes raising the temperature to  $75^{\circ}\text{C}$ , where the DNA polymerases catalyze the synthesis of the complementary DNA strands by extending the primers using deoxynucleotide triphosphates (dNTPs) as building blocks. Natural convection PCR devices exhibit continuous denaturation and renaturation as reactants circulate through distinct reaction zones. Consequently, the concentration dynamics of ssDNA ( $S_1$  and  $S_2$ ) and dsDNA ( $S_1S_2$ ) in our simulations are anticipated to be similar to the fluorescence intensity behavior observed in quantitative PCR (qPCR) tests.

Quantitative PCR (qPCR) enables the measurement of amplicon accumulation over time by monitoring the fluorescence intensity generated by fluorophores incorporated into the reaction. The fluorescence intensity is directly proportional to the concentration of the amplified DNA. The behavior of the fluorescence intensity during qPCR typically exhibits four distinct phases (Fig. 2), which include an initial stage (basal phase) with minimal fluorescence (baseline signal) before target DNA amplification begins [18]. In the second stage (exponential phase), the fluorescence intensity increases exponentially as target DNA amplification progresses

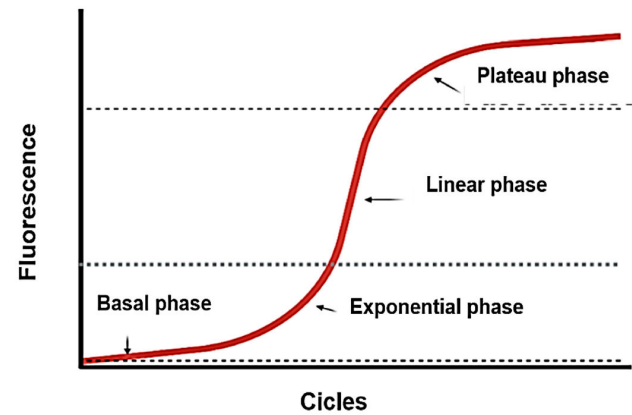


FIGURE 2. The qPCR technique allows the measurement of the concentration of the amplified DNA during a PCR experiment by measuring the fluorescence emitted during the sequential cycles of the process. The first of the four phases is the basal one, corresponding to the signal before target DNA amplification begins. The exponential signal (second phase) is due to the rapid progress of fluorescence intensity of target DNA amplification. The linear phase (third stage) indicates a constant rate of amplicon generation. The plateau (final phase), with fluorescence maximum intensity, corresponds to the end point of amplification. Adapted image from [17].

rapidly. The linear phase (third stage) involves a steady and linear increase in fluorescence intensity, indicating a constant rate of amplicon generation. The final stage corresponds to the plateau phase, where the fluorescence intensity reaches a maximum, signaling the end point of amplification.

This work proposes a methodology framework for simulating and optimizing reaction kinetics in natural convection microfluidic devices using computer simulation and a multi-physics approach. The approach involves coupling heat and mass transfer, fluid flow, and chemistry of the reactants. Visual and regression analyses are performed to evaluate the impact of different operational parameters on reaction speed, aiming to improve microfluidic natural convection systems. The proposed methodology is applied to a PCR microfluidic device that utilizes natural convection for the required reactions.

## 2. Methodology

The proposed methodology aims to simulate and analyze the effects of several operational parameters on natural convection devices. Then, it is crucial to establish the operational parameters, experimental and device designs, and meshing applied. To describe the experiment, we consider mathematical models that describe fluid motion, temperature distribution, species transport, and reaction kinetics. Once these models are defined, analyzing the simulation results and identifying relevant variables of interest involves conducting visualization and regression analyses to assess the impact of operational parameters on the reaction rate and optimize it accordingly.

## 2.1. Methodology software

COMSOL Multiphysics (ver. 5.3.) was used to simulate a PCR microfluidic device. It is a finite element-based simulation platform capable of simulating fully coupled multi-physics and single-physics phenomena. Nevertheless, other multi-physics simulation software could be used similarly.

## 2.2. Operational parameters and experiment design

Using pumps is not feasible since we are dealing with natural convection devices. Therefore, a constant temperature gradient is generated to induce a mass flux within the device. This temperature gradient leads to density variations in the fluid, leading to a mass flux driven by the force of gravity. Based on this principle, the operational parameters required to generate a mass flux and promote adequate mixing and reactions among different chemical species include the inner diameters of the devices and fixed temperatures at various locations within the device. By manipulating these parameters, optimal conditions for efficient and accelerated mixing and reactions can be determined. Furthermore, the design and materials of the device can be considered as additional parameters, treated as categorical variables, to evaluate their impact through regression analysis. This type of analysis aids in selecting the appropriate material and design for fabricating the device. It is recommended to establish a complete or fractional factorial design for the simulations to investigate the impact of different parameters on the rate of chemical reactions through a regression analysis. The results of the simulations and the operational parameters will be used to perform visual and regression analyses to evaluate the individual effects of each parameter.

The application of the methodology in this work focuses on a PCR device that relies on natural convection. The operational parameters for this PCR device include three specific temperatures: 1) the denaturing temperature (TD), 2) the annealing temperature (TA), and 3) the extension temperature (TE). The values were selected to cover the typical experimental PCR ranks. Additionally, the inner diameter (ID) of the device is considered an operational variable, and the corresponding values for all parameters can be found in Table I. A complete  $3^4$ -factorial design was used, considering the 81 possible combinations of the parameters listed in Table I, to measure the influence of the parameter on the rate of PCR reactions.

TABLE I. Operational parameters of PCR device.

TD (°C)	TA (°C)	TE (°C)	ID ( $\mu\text{m}$ )
92	55	70	632.4
95	60	72	690.8
98	65	74	797.5

TD, TA, and TE temperatures were based on [14,15]. Internal diameters ID were taken from [16].

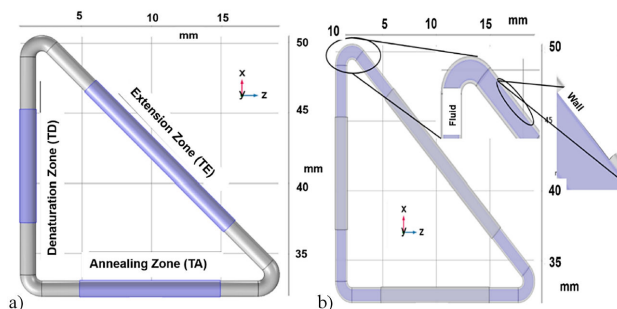


FIGURE 3. a) Isothermal temperature constraints: denaturation zone (TD), annealing zone (TA), and extension zone (TE). b) Domains of the PCR system: fluid and walls.

TABLE II. Finer mesh properties correspond to three different inner diameter capillary tubes.

Variable	Value		
Capillary ID ( $\mu\text{m}$ )	632.4	690.8	797.5
Number of domain elements	428,492	164,770	519,643
Number of vertex elements	60	60	60
Number of edge elements	3,694	2,136	3,600
Number of boundary elements	108,786	33,136	122,760
Number of elements	411,358	148,873	502,855
Free meshing time (s)	11.88	6.14	13.59
Minimum element quality (ua)	0.1937	0.228	0.1749

## 2.3. Device design and meshing

The proposed PCR device design was imported to COMSOL. It was a capillary glass tube shaped like a closed triangular loop with a length of 64 mm [Fig. 3a)]. The CAD models of the device were created using AutoCAD<sup>®</sup>. The diameters are specified in Table I. The device is divided into two domains [Fig. 3b)]. The inner section of the tube was filled with a liquid (in this case, water), where the chemical species will be present and undergo reactions. In contrast, the outer section of the tube is a solid material (in this case, borosilicate glass).

An automatic finer mesh was applied to the imported models into COMSOL. The mesh selection was based on the consideration that larger meshes resulted in warnings or errors within the program. In contrast, smaller meshes did not yield significant changes in the simulations. The properties of the three meshes generated can be found in Table II.

## 2.4. Mathematical models

### 2.4.1. Fluid model

The modeling of fluid motion relies on utilizing the steady-state Navier-Stokes Eqs. (1) and the continuity Eq. (2). Gravitational force and temperature-dependent density changes are considered. The inertial term of the Navier-Stokes equa-

TABLE III. Proportionality factors of (10)-(14) equations.

Species	Parameters
$k_0^+$	$12.5 \text{ s}^{-1}$
$k_0^-$	$10^6 \text{ M}^{-1} \text{ s}^{-1}$
$k_1^+$	$5 * 10^6 \text{ M}^{-1} \text{ s}^{-1}$
$k_1^-$	$10^{-4} \text{ s}^{-1}$
$k_2$	$0.32 \text{ s}^{-1}$

tions is neglected due to the scale of the system under consideration [20].

$$\nabla \cdot (\mu \nabla \mathbf{u} + \mu \nabla^T \mathbf{u}) - \nabla \cdot \left( \frac{2}{3} \mu I \nabla \mathbf{u} \right) - \nabla p + \rho \mathbf{g} = 0, \quad (1)$$

$$\nabla \cdot (\rho(\mathbf{r}) \mathbf{u}(\mathbf{r})) = 0, \quad (2)$$

where  $\mathbf{u}$  is the velocity vector,  $\rho$  is the density of the fluid,  $\mu$  is the dynamic viscosity, and  $p$  is the pressure. All simulations enforced a boundary no-slip condition, with stationary walls and an initial state of water at rest. The system was set to an initial temperature of 20°C and a pressure of 1 atm.

#### 2.4.2. Thermal model

The modeling of heat transfer is based on the steady-state heat Eq. (3),

$$-\kappa \nabla^2 T(\mathbf{r}) + C_p \rho(\mathbf{r}) \mathbf{u}(\mathbf{r}) \cdot \nabla T(\mathbf{r}) = \sum_j Q_j \quad (3)$$

where  $C_p$  is the specific heat capacity,  $T$  is the temperature,  $\kappa$  is the thermal conductivity,  $\mathbf{u}$  is the velocity field of the fluid, and  $Q_j$  is the rate of heat generated in the device [21]. As was described before, for the specific practical example under consideration, the system was divided into three constant temperature zones (TD, TA, and TE) located at specific sections of the walls [Fig. 3a)]. Each zone corresponds to the temperature required for PCR reactions: denaturation, annealing, and extension (Table III).

#### 2.4.3. Transport of species model

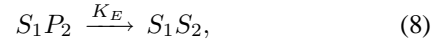
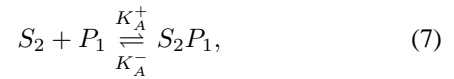
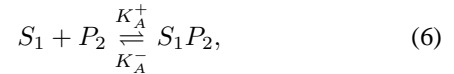
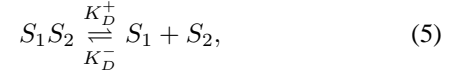
Species transport utilizes the time-dependent transport Eq. (4), which incorporates convection.

$$\partial_t c_i(\mathbf{r}, t) - D_i \nabla^2 c_i(\mathbf{r}, t) + \mathbf{u}(\mathbf{r}) \cdot \nabla c_i = \sum_j Q_j \quad (4)$$

where  $c_i$  is the concentration,  $D_i$  is the diffusion coefficient,  $t$  is the time,  $\mathbf{u}$  is the velocity field of the fluid,  $i$  is a chemical species, and  $Q_j$  is the production rate of the species  $i$  in the device, calculated on a provided reaction kinetics model [21].

#### 2.4.4. Kinetics Model

Several kinetics models can be inputted into the software to simulate the corresponding kinetics. These models can be either independent or dependent on the temperature of the system. The goal is to achieve proper mixing and reactions among the species. The temperature-dependent kinetics model used in this work [10,11] considers five chemical species that describe denaturing, renaturing, annealing, reverse annealing, and extension processes, describe for Eqs. (5)-(9)



The chemical species  $S_1 S_2$  are the dsDNA,  $S_1$  and  $S_2$  represent the mutually complementary ssDNA pair, whereas  $S_1 P_2$  and  $S_2 P_1$  are the primer-ssDNA complexes. The corresponding reaction coefficients are  $k_D^+$  for denaturing,  $k_D^-$  for renaturing,  $k_A^+$  for annealing,  $k_A^-$  for reverse annealing, and  $k_E$  for extension. Reaction rates are given by Eqs. (10)-(14)

$$K_D^+(T) = \frac{k_0^+}{2} \left( 1 + \tanh \left[ \frac{T - 88}{5} \right] \right), \quad (10)$$

$$K_D^-(T) = \frac{k_0^-}{2} \left( 1 + \tanh \left[ -\frac{T - 75}{5} \right] \right), \quad (11)$$

$$K_A^+(T) = \frac{k_1^+}{2} \left( 1 + \tanh \left[ -\frac{T - 62.5}{5} \right] \right), \quad (12)$$

$$K_A^-(T) = \frac{k_1^-}{2} \left( 1 + \tanh \left[ \frac{T - 66}{5} \right] \right), \quad (13)$$

$$K_E(T) = k_2 \exp \left( - \left[ \frac{T - 70}{5} \right]^2 \right), \quad (14)$$

where  $T$  is the temperature in Kelvin and  $k_0^+$ ,  $k_0^-$ ,  $k_1^+$ ,  $k_1^-$ , and  $k_2$  are proportionality factors defined in Table III.

#### 2.5. Simulation process

The properties of the different species, including initial concentrations and diffusivity constants, are defined in Table IV.

The simulation process is divided into two primary parts: 1) a steady-state analysis of the termofluidic fields within the device and 2) a time-dependent analysis of the transport and chemical reactions among the different chemical species. Separating simulations into stationary and time-dependent

TABLE IV. Chemical species parameters ( $S_1S_2$ ,  $S_1$ ,  $S_2$ ,  $P_1$ ,  $P_2$ ,  $S_1P_2$ , and  $S_2P_1$ ) and their diffusion coefficients. Taken from [11].

Species	Parameters	
	Diffusion coefficient $D_i \times 10^9, (\text{m}^2\text{s}^{-1})$	Initial concentration $c_i (\text{M})$
$S_1, S_2$	1	0
$P_1, P_2$	10	$3e-5$
$S_1P_2, S_2P_1$	10	0
$S_1S_2$	10	$5.71e^{-10}$

parts simplifies computations and reduces the required computational resources and time. All the mathematical models treated need to be configured in the software along with the boundary and initial conditions. The first study involves calculating the velocity and temperature fields within the device. This was achieved by coupling the Creeping flow, Heat transfer in fluids, and Non-isothermal flow modules. A parametric sweep can be configured to conduct simulations with varying combinations of operational parameters. The average fluid velocity (AvgVel) was computed for each simulation. The second study involves calculating the reaction kinetics of the reactions over time, ranging from 0 to 60 minutes with 1-minute steps. These values could be modified depending on the computing capacities and the accuracy needed. It was achieved by coupling the chemistry and transport of diluted species modules and using the velocity and temperature fields obtained from the first study to calculate the reactions among the chemical species and their corresponding concentrations at each time step. For the PCR device example, the simulations were performed using the complete factorial design with the parameters in Table IV.

## 2.6. Processing and analysis of the simulation results

The simulations provide valuable information, including the total reaction time (RTIME). However, in the case of the PCR reactions presented as a practical example, we can also calculate additional variables of interest. These variables include the duration of the exponential phase of the reactions (EXPTIME) and the slope of the logarithm of the normalized concentration of  $S_1S_2$  (SlopeLog-dsDNA) or  $S_1$  and  $S_2$  (SlopeLog-ssDNA) during the exponential phase. These additional variables are significant as they indicate the suitability of the parameters for one phase, which can extend to subsequent phases. Moreover, the operational parameters, the temperature differences TD-TA, TD-TE, and TE-TA, and the average fluid velocity (AvgVel) are also variables of interest. Once the variables of interest have been collected, a visual analysis of data allows comparison of the different variables to identify those that exhibit a higher degree of explanatory power for a regression analysis. By selecting the most influential variables, we can effectively explain the speed of the

reactions. Then, a regression analysis will be conducted to describe the speed of the reactions and quantify the influence of each parameter on the reaction rate.

## 2.7. Computer specifications

Simulations were performed on a 2019 Acer Predator Helios 300 laptop with 16GB of RAM, an Intel i7-9750H processor, Windows 11 home OS, NVidia GTX 1660Ti graphics card, and x64 architecture.

## 3. Numerical results and discussion

### 3.1. Simulation results

The methodology implemented can predict how temperature gradients in natural convection devices affect fluid motion and reaction kinetics in a given problem. We used a PCR to exemplify the application of a natural convection device, with 81 simulations conducted. Table V presents the TD, TA, TE, and ID parameters and AvgVel, Slope\_Log\_dsDNA, EXPTIME, and RTIME calculations obtained from the 50 simulations that converged. TD, TA, TE, and ID were selected between the lower and higher values considered in an experimental PCR. All stationary analyses converged except for the time-dependent analyses, where sudden negative and infinite concentrations appeared, possibly due to internal calculation errors like rounding decimals, mesh quality, or the magnitude of time steps. The obtained reaction times ranged from 18 to 21 minutes, notably shorter than traditional PCR devices, where reaction times typically range from 30 to 40 minutes [8].

Figure 4 illustrates the velocity and temperature profiles within the PCR device for simulation SIM78, with TD = 98°C, TA = 65°C, TE = 74°C, and ID = 797.5  $\mu\text{m}$ . The velocity profile [Fig. 4a)] shows a parabolic-like behavior, satisfying the no-slip boundary condition. The temperature profile [Fig. 4b)] indicates the fluid flow direction, which extends from the denaturation zone (TD zone) to the extension zone (TE zone) and ultimately to the annealing zone (TA zone). These characteristics hold for the remaining stem simulation as well. However, the current direction of fluid flow is a problem as it slows down the reaction rate. Ideally, the fluid should flow from the denaturation zone (TD zone) to the

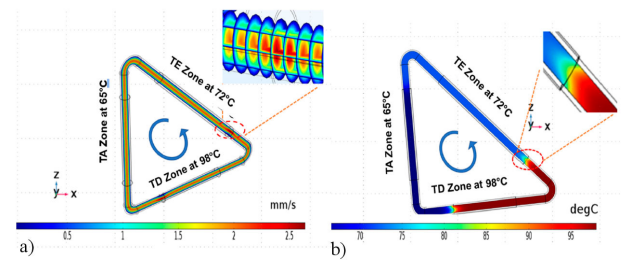


FIGURE 4. a) Velocity and b) temperature profile from the simulation SIM78 (ID = 797.5  $\mu\text{m}$ , TD = 98°C, TA = 65°C, and TE = 72°C).

TABLE V. TD, TA, TE, and ID parameters and calculations AvgVel, Slope\_Log\_dsDNA as SLOPE, EXPTIME, and RTIME from the converged PCR system.

SIM	TD (°C)	TA (°C)	TE (°C)	ID ( $\mu\text{m}$ )	AvgVel (mm/s)	SLOPE (1/min)	EXPTIME (min)	RTIME (min)
Sim 2	92	55	70	690.8	0.928	0.174	21.463	28.831
Sim 3	92	55	70	797.5	1.248	0.216	15.622	22.975
Sim 5	92	55	72	690.8	1.000	0.195	18.783	24.876
Sim 6	92	55	72	797.5	1.341	0.229	16.527	22.890
Sim 7	92	55	74	632.4	0.901	0.204	17.830	23.981
Sim 8	92	55	74	690.8	1.074	0.226	16.520	22.971
Sim 12	92	60	70	797.5	1.018	0.185	18.787	26.873
Sim 15	92	60	72	797.5	1.114	0.203	18.382	25.979
Sim 17	92	60	74	690.8	0.903	0.203	18.747	24.877
Sim 18	92	60	74	797.5	1.212	0.231	15.718	22.818
Sim 19	92	65	70	632.4	0.447	0.130	27.209	45.565
Sim 20	92	65	70	690.8	0.545	0.135	25.936	41.994
Sim 22	92	65	72	632.4	0.518	0.131	25.264	42.668
Sim 23	92	65	72	690.8	0.625	0.137	26.861	42.653
Sim 25	92	65	74	632.4	0.587	0.136	27.281	42.755
Sim 30	95	55	70	797.5	1.328	0.243	13.717	20.963
Sim 32	95	55	72	690.8	1.059	0.200	17.577	24.964
Sim 33	95	55	72	797.5	1.423	0.266	14.617	20.922
Sim 34	95	55	74	632.4	0.950	0.220	15.655	21.892
Sim 35	95	55	74	690.8	1.134	0.251	14.591	20.892
Sim 39	95	60	70	797.5	1.098	0.201	19.671	26.998
Sim 42	95	60	72	797.5	1.196	0.207	16.776	23.791
Sim 45	95	60	74	797.5	1.295	0.254	13.966	20.901
Sim 46	95	65	70	632.4	0.495	0.138	22.765	40.884
Sim 47	95	65	70	690.8	0.602	0.142	26.110	40.823
Sim 48	95	65	70	797.5	0.829	0.160	21.347	35.813
Sim 49	95	65	72	632.4	0.565	0.132	26.518	41.720
Sim 50	95	65	72	690.8	0.683	0.146	24.497	41.806
Sim 51	95	65	72	797.5	0.931	0.170	21.701	36.567
Sim 52	95	65	74	632.4	0.635	0.139	24.770	39.844
Sim 53	95	65	74	690.8	0.763	0.150	26.562	39.795
Sim 57	98	55	70	797.5	1.411	0.226	15.947	21.864
Sim 59	98	55	72	690.8	1.120	0.204	18.733	24.856
Sim 60	98	55	72	797.5	1.508	0.251	12.917	19.986
Sim 61	98	55	74	632.4	1.001	0.215	16.713	22.981
Sim 62	98	55	74	690.8	1.196	0.238	14.491	20.880
Sim 63	98	55	74	797.5	1.606	0.282	13.756	18.998
Sim 64	98	60	70	632.4	0.722	0.150	24.592	32.849
Sim 66	98	60	70	797.5	1.182	0.212	17.886	25.820
Sim 69	98	60	72	797.5	1.281	0.217	15.787	23.867
Sim 72	98	60	74	797.5	1.381	0.245	13.784	20.995
Sim 73	98	65	70	632.4	0.544	0.135	25.489	41.428
Sim 74	98	65	70	690.8	0.662	0.153	24.586	41.596
Sim 75	98	65	70	797.5	0.912	0.177	20.846	34.946
Sim 76	98	65	72	632.4	0.615	0.140	24.512	41.656
Sim 77	98	65	72	690.8	0.743	0.150	21.913	36.409
Sim 78	98	65	72	797.5	1.016	0.167	21.592	37.828
Sim 79	98	65	74	632.4	0.686	0.148	22.290	37.499
Sim 80	98	65	74	690.8	0.825	0.147	26.648	39.512
Sim 81	98	65	74	797.5	1.120	0.161	21.626	33.887

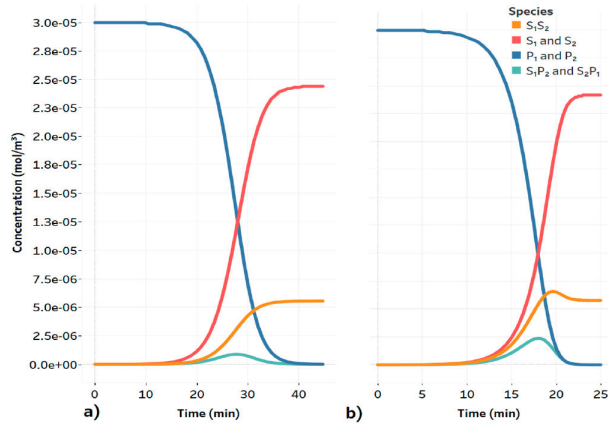


FIGURE 5. Kinetics of the PCR reactions of the chemical species of selected simulations. a) SIM3 with parameters  $ID = 797.5 \mu\text{m}$ ,  $TD = 92^\circ$ ,  $TA = 55^\circ$ , and  $TE = 70^\circ$  and b) SIM78 with parameters  $ID = 797.5 \mu\text{m}$ ,  $TD = 98^\circ$ ,  $TA = 65^\circ$ , and  $TE = 72^\circ$ .

annealing zone (TA zone) and then to the extension zone (TE zone). This directional issue is due to the geometry of the system and the positioning of the temperature constraints.

Figures 5 show the reaction kinetics in two simulations, SIM3 [Figs. 5a)],  $ID = 797.5 \mu\text{m}$ ,  $TD = 92^\circ\text{C}$ ,  $TA = 55^\circ\text{C}$ , and  $TE = 70^\circ\text{C}$  and SIM78 [Figs. 5b)],  $ID = 797.5 \mu\text{m}$ ,  $TD = 98^\circ\text{C}$ ,  $TA = 65^\circ\text{C}$ , and  $TE = 72^\circ\text{C}$ ], presenting continuous processes of denaturation and renaturation. This characteristic holds for the remaining simulations as well. For SIM3, the concentration of dsDNA ( $S_1S_2$ ) and ssDNA ( $S_1$  and  $S_2$ ) were similar to the fluorescence intensity observed in qPCR tests, whereas SIM78 showed denaturation and renaturation rates exhibiting variations over a time interval with a decrease in dsDNA ( $S_1S_2$ ) concentration at certain time intervals. It can be attributed to a fast amplification rate that exceeded the denaturation rate until the reactants were sufficiently depleted to reduce the amplification rate, allowing the denaturation process to enter a more pronounced plateau phase.

### 3.2. Target variable selection

Minimizing the total reaction time (RTIME) is needed to increase specific reaction rates. Other significant variables in PCR reactions include the duration of the exponential phase (EXPTIME) and the slope of the logarithm of the normalized concentration of dsDNA ( $S_1S_2$ ) during the exponential phase (SlopeLog-dsDNA).

These variables provide insights into the suitability of parameters for one phase, which can extend to subsequent phases (Fig. 6). Figure 6a) displays the positive correlation between EXPTIME and RTIME, while Fig. 6b) exhibits the negative correlation between EXPTIME and SlopeLog-dsDNA. Then, there is also a negative correlation between RTIME and SlopeLog-dsDNA. Consequently, it is necessary to maximize SlopeLog-dsDNA or minimize RTIME or EXPTIME. A regression analysis was performed after selecting one of these variables as a response to the system. A his-

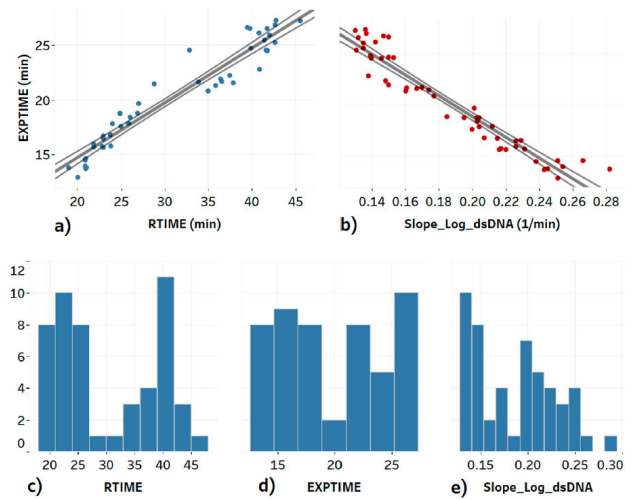


FIGURE 6. Correlation between response variables of the PCR system: a) EXPTIME vs RTIME and b) EXPTIME vs Slope\_Log\_dsDNA. Frequency distribution of the response variables: c) RTIME, d) EXPTIME, and e) Slope\_Log\_dsDNA.

to-gram of the three mentioned variables was plotted to make the proper selection [Figs. 6c) for RTIME, 6d) for EXPTIME, and 6e) Slope\_Log\_dsDNA]. EXPTIME was chosen because it is closer to a constant distribution than the other two variables, which is useful when a simple regression is applied.

## 4. Visual analysis

An essential factor in a natural convection device is the flow velocity caused by density differences resulting from temperature variations. A higher temperature difference leads to more significant density differences, making liquid displacement easier and faster. This relationship is shown in Fig. 7a), presenting a positive correlation between AvgVel and the temperature difference (TD-TA). Similarly, Fig. 7b)

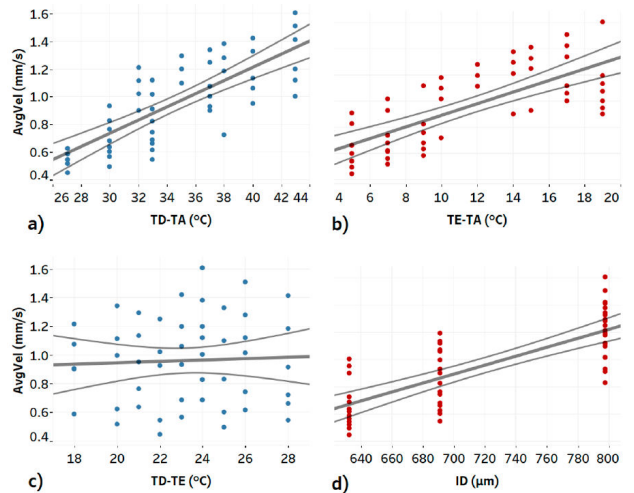


FIGURE 7. Correlation between different PCR system variables from the simulations. a) AvgVel vs TD-TA, b) AvgVel vs TE-TA, c) AvgVel vs TD-TE, and d) AvgVel vs ID.

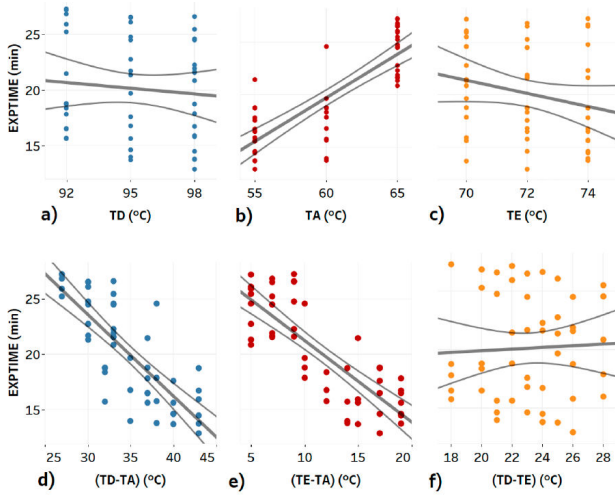


FIGURE 8. Correlation between different PCR system variables from the simulations. a) EXPTIME vs TD, b) EXPTIME vs TA, c) EXPTIME vs TE, d) EXPTIME vs TD-TA, e) EXPTIME vs TE-TA, and f) EXPTIME vs TD-TE.

exhibits a positive correlation between AvgVel and the temperature difference (TE-TA). However, in Fig. 7c), although a weak positive correlation is observed between AvgVel and the temperature difference (TD-TA), it could be negligible due to the scattered distribution of points around the trend line. In addition, Fig. 7d) shows a positive correlation between ID and AvgVel, indicating that liquid flow is facilitated in larger spaces.

Figures 8a) and 8c) show a negative correlation between EXPTIME and temperatures TD and TE, respectively. In contrast, Fig. 8b) shows a positive correlation between EXPTIME and temperature TA. This relationship is supported by Fig. 8d) and 8e), where a negative correlation is observed between EXPTIME and temperature differences (TD-TA) and (TE-TA), respectively, opposite to the observed between AvgVel and those temperature differences. Moreover, the correlation between (TD-TE) and EXPTIME [Fig. 8f)] is negligible, similar to the relationship between AvgVel and (TD-TE). In addition, it is shown that (TD-TA) and (TE-TA) have a higher incidence on EXPTIME than the individual temperatures TD, TE, and TA.

In Fig. 9a), a negative correlation is observed between EXPTIME and ID, opposite to the correlation between AvgVel and ID [Fig. 7d)]. Then, increasing the temperature differences (TD-TA) and (TE-TA) leads to an increase in the average velocity of the fluid (AvgVel) due to the increase of the density differences in the fluid caused by those temperature differences, see Figs. 7 and 8. Consequently, the increase in AvgVel decreases EXPTIME, which aligns with our objective of optimizing a natural convection device. This relationship is highlighted in Fig. 9b), demonstrating a negative correlation between AvgVel and EXPTIME. This reinforces the importance of temperature differences in influencing fluid velocity (AvgVel) and the subsequent reduction of EXPTIME.

In summary, the variables with the most significant incidence on the target variable EXPTIME are the temperature

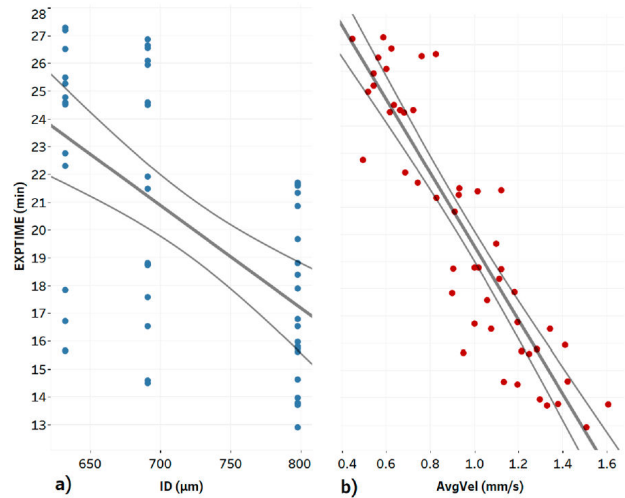


FIGURE 9. Correlation between different PCR system variables from the simulations. a) EXPTIME vs ID and b) EXPTIME vs AvgVel.

differences (TD-TA) and (TE-TA) and the inner diameter ID because they are strongly associated. This can be attributed to the relationship between the temperature differences and the inner diameter with the average velocity (AvgVel) and the relationship between AvgVel and EXPTIME. Increasing the temperature differences (TD-TA) and (TE-TA), as well as the inner diameter ID, causes an increase in AvgVel. Consequently, the increase in AvgVel causes a decrease in EXPTIME. It means that in the PCR device, the renaturation and reverse annealing, along with the direction of fluid flow, contribute to the deceleration of reactions. However, this deceleration can be mitigated by increasing fluid flow velocity. To measure the impact of parameters on the variable EXPTIME, a regression analysis was applied with the most influential variables: (TD-TA), (TE-TA), and ID. Considering the available data and its behavior, a simple linear regression is sufficient for measuring the impact of each parameter on EXPTIME.

#### 4.1. Regression analysis

The (TD-TA), (TE-TA), and ID data were standardized for the regression analysis by subtracting the mean and dividing by the standard deviation to visualize the regression residuals. The resulting model corresponds to Eq. (15)

$$EXPTIME = -1.015(TD - TA) - 2.484(TE - TA) - 1.912ID + 20.118, \quad (15)$$

where the temperature difference (TD-TA) is the most significant parameter, followed by the inner diameter ID and the temperature difference (TE-TA), respectively. To minimize EXPTIME, TA temperature should be decreased, thereby simultaneously increasing (TD-TA) and (TE-TA) temperature differences. Also, we have the flexibility to manipulate the TD and TE temperatures for better control over the process.

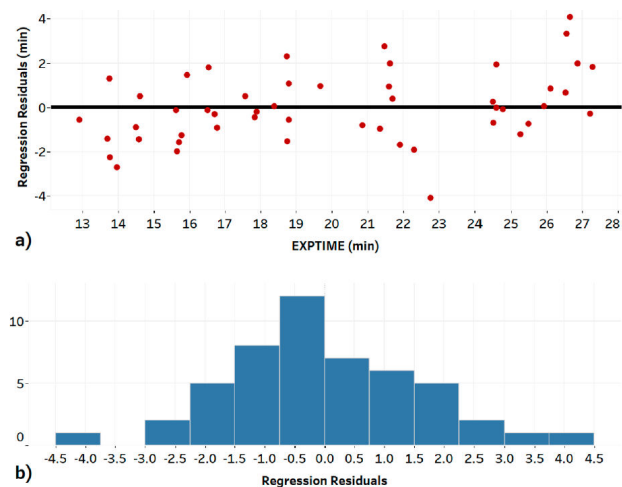


FIGURE 10. Residuals distribution of the EXPTIME vs (TD-TA), (TE-TA), and ID regression. a) Scatterplot of the regression residuals and b) frequency distribution of the residuals.

Figure 10a) shows a scatterplot of the residuals with no discernible pattern indicating any regression issues and, for instance, a reliable regression model. Figure 10b) shows a histogram of the residuals, which shows a closer normal shape distribution, considered acceptable in the analysis context.

Nevertheless, the natural convection PCR has certain limitations, especially regarding the TD temperature. Going beyond  $98^{\circ}\text{C}$  can result in the degradation of chemical components in real-life applications. However, we can still optimize the reaction rates by adjusting the parameters ID, TE, and TA. Another approach is reducing the heating area size (TD zone) to minimize the time available for potential chemical degradation, potentially allowing it to surpass the  $98^{\circ}\text{C}$  limit. Despite the challenges of the fluid flow direction and the rates of renaturation and reverse annealing, the regression analysis allows us to quantify the influence of several parameters in the system. Then, through this analysis, we can get insights into mitigating these undesirable effects and enhancing the

overall system performance. Moreover, the developed model helps to optimize the PCR natural convection system. However, further enhancements can be achieved by incorporating multiple designs or materials as parameters (categorical variables) to quantify the benefits of different designs or materials and make informed decisions based on their effectiveness.

## 5. Conclusions

A methodology was proposed and applied to a natural convection PCR device with a multi-physics approach to solving the fluid flow direction that leads to slower reactions. The visual and regression analyses help to increase reaction rates despite the effects of flow direction. Our findings revealed that fluid flow velocity is essential in determining the reaction speed, which could be controlled by adjusting the temperature differences (TD-TA) and (TE-TA), as well as the inner diameter ID of the device. These temperature differences were found to have more significant importance than the individual temperatures. The temperature differences showed no correlation with the reaction kinetics speed. Despite the challenges posed by the fluid flow direction, the best reaction times achieved ranged from 18 to 21 min. This indicates that a different design, with an appropriate fluid flow direction, can further improve reaction times by implementing visual and regression analyses to gain insights into the control of different operational parameters. An advantage of this methodology framework is that it allows simulations on mid-range computers due to the null requirement of a discrete graphics card, the considered simplifications, and the mesh size. Also, it allows the determination of the impact of several parameters on the rate of reaction kinetics in microfluidic natural convection devices, therefore providing valuable insights for device improvement. In the same way, multiple designs could be treated as a variable to measure the impact of a particular design, helping in the development of robust device designs.

1. T. Han *et al.*, Recent advances in detection technologies for COVID-19 (2021), <https://doi.org/10.1016/j.talanta.2021.122609>.
2. D. Sidransky, Nucleic acid-based methods for the detection of cancer (1997), <https://doi.org/10.1126/science.278.5340.1054>.
3. J. W. Allen, M. Kenward, and K. D. Dorfman, Coupled flow and reaction during natural convection PCR, *Microfluidics and Nanofluidics* **6** (2009) 121
4. N. Agrawal, Y. A. Hassan, and V. M. Ugaz, A Pocket-Sized Convective PCR Thermocycler, *Angewandte Chemie* **119** (2007) 4394, <https://doi.org/10.1002/ange.200700306>.
5. C. D. Ahrberg, A. Manz, and B. G. Chung, Polymerase chain reaction in microfluidic devices, *Lab on a Chip* **16** (2016) 3866
6. Microfluidics: Applications for analytical purposes in chemistry and biochemistry (2007), <https://doi.org/10.1002/elps>.
7. Z. Sheidaei, P. Akbarzadeh, and N. Kashaninejad, Advances in numerical approaches for microfluidic cell analysis platforms (2020), <https://doi.org/10.1016/j.jsamd.2020.07.008>.
8. M. M. A. Bhutta *et al.*, CFD applications in various heat exchangers design: A review (2012), <https://doi.org/10.1016/j.applthermaleng.2011.09.001>.
9. A. Hassibi, H. Kakavand, and T. H. Lee, A stochastic model and simulation algorithm for polymerase chain reaction (PCR) systems.
10. V. E. Papadopoulos *et al.*, Comparison of continuous-flow and static-chamber micro-PCR devices through a computational

- study: the potential of flexible polymeric substrates, *Microfluidics and Nanofluidics* **19** (2015) 867, <https://doi.org/10.1007/s10404-015-1613-1>.
11. M. Laudon *et al.*, Multi-physics Simulation Analysis of a Novel PCR Micro-Device (Nano Science and Technology Institute, 2007).
  12. A. Priye, Y. A. Hassan, and V. M. Ugaz, Microscale chaotic advection enables robust convective DNA replication, *Analytical Chemistry* **85** (2013) 10536, <https://doi.org/10.1021/ac402611s>.
  13. S. Raasch and D. Etling, Modeling Deep Ocean Convection: Large Eddy Simulation in Comparison with Laboratory Experiments.
  14. J. M. S. Bartlett and D. Stirling, Methods in Molecular Biology TM Methods in Molecular Biology TM PCR Protocols second edition Edited by PCR Protocols.
  15. M. A. Innis, PCR protocols: a guide to methods and applications (Academic Press, 1990), p. 482.
  16. P. Turnpenny and S. Ellard, Emery's ELEMENTS of MEDICAL GENETICS, 15th ed. (ELSEVIER, 2017).
  17. Biorender, <https://app.biorender.com/>.
  18. M. Arya *et al.*, Basic principles of real-time quantitative PCR (2005), <https://doi.org/10.1586/14737159.5.2.209>.
  19. Kimble® Microcaps® Capillary Tube — DWK Life Sciences, <https://www.dwk.com/na/kimble-microcaps-capillary-tube>.
  20. H. Bruus, Theoretical microfluidics, **vol. 18** (Oxford university press, 2007).
  21. H. D. H. D. Baehr and K. K. Stephan, Heat and mass-transfer (Springer, 2006), p. 688.
  22. M. Krishnan *et al.*, Reactions and fluidics in miniaturized natural convection systems, *Analytical Chemistry* **76** (2004) 6254, <https://doi.org/10.1021/ac049323u>.